ACS Sustainable Resource Management

pubs.acs.org/acssrm

Article

Tailoring KOH-Activated Hydrochar Derived from Sugarcane Industry By-Products through an Adsorption Study with Fipronil

Gabriela A. Nogueira, Márcio J. Laranja, Suelen A. Mondek, Laís H. S. Vieira, Mauricio Boscolo, Odair P. Ferreira, Altair B. Moreira, and Márcia C. Bisinoti*

Cite This: ACS Sustainable Resour. Manage. 2025, 2, 1977−1985

Read Online

ACCESS | Metrics & More | Article Recommendations | Supporting Information

ABSTRACT: Rising food demand has intensified pesticide use, notably fipronil, raising concerns over soil and water contamination. Hydrochars (HC) were synthesized from sugarcane bagasse and vinasse via hydrothermal carbonization (HTC) with H_3PO_4, followed by thermochemical activation with KOH at 500 and 700 °C using HC:KOH ratios of 1:2 and 1:4, yielding four activated hydrochars (AHC-5-2, AHC-5-4, AHC-7-2, AHC-7-4) for fipronil adsorption. HC and AHCs were characterized for composition, structure, morphology, textural properties, and surface functional groups. Activation at 500 °C reduced the carbon content of HC from 77.0% to 52.3% (1:2) and 56.5% (1:4), whereas at 700 °C it decreased to 34.4% (1:2) and 67.6% (1:4). KOH activation removed inorganic matter, decreased the diffraction peaks, and reduced acidic and phenolic groups. AHC-7-4 exhibited the highest surface area (870 $m^2\ g^{-1}$) and micropore fraction (71−82%), achieving maximal fipronil adsorption (249 mg g^{-1} in 300 min), predominantly controlled by diffusion and chemical interactions. Overall, thermochemical activation markedly enhanced HC adsorption, particularly under high-temperature and high-ratio conditions, underscoring the sustainable potential of these materials for pesticide remediation.

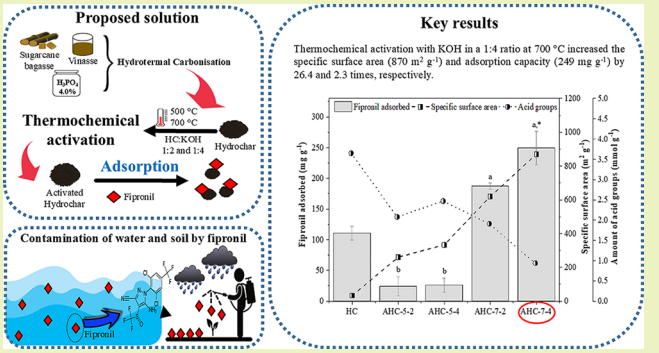

KEYWORDS: *thermochemical activation, insecticides, hydrochar, biomass, environmental application*

1. INTRODUCTION

Population growth has intensified pesticide use to enhance agricultural productivity.[1−3] Fipronil (5-amino-1-[2,6-dichloro-4-(trifluoromethyl)phenyl]-4-[(trifluoromethyl)sulfinyl]-1*H*-pyrazole-3-carbonitrile), a broad-spectrum insecticide extensively applied in Brazilian sugarcane cultivation, has raised concerns due to risks of soil and water contamination from inadequate disposal and storage.[4−7] Its cytotoxic, reproductive, hepatotoxic, and neurotoxic effects on humans, animals, bees, and plants are well documented.[2,8−11] Accordingly, research has focused on sustainable remediation strategies, particularly through materials derived from biomass by-products.[12−14] Such approaches support the United Nations sustainable development goals (SDGs), notably, SDG 6 (Clean Water and Sanitation), SDG 12 (Responsible Consumption and Production), and SDG 13 (Climate Action).

Hydrochars (HCs) are synthesized via hydrothermal carbonization (HTC), a process increasingly studied for its adaptability, simplicity, reliance on renewable feedstocks, and operation at relatively mild temperatures (180−260 °C).[15] Our group[16−20] has prepared HCs from sugarcane bagasse and vinasse using phosphoric acid (H_3PO_4) as an additive, which promotes phosphate group incorporation, thereby improving adsorption capacity and simultaneously providing a potential nutrient source when applied to soils.[21,22] This strategy enables solubilization or suspension of biomass and additives in water, facilitating milder reaction conditions and broader precursor flexibility.[17,23] The valorization of agro-industrial residues through HTC aligns with circular economy principles and advances SDG 9 (Industry, Innovation and Infrastructure) and SDG 15 (Life on Land).

HC has been studied for its metal-chelating ability, particularly Cu^{2+}, through interactions with humic-like substances and as a soil conditioner.[16] These findings highlight its dual role in soil remediation and as a source of nutrients and organic carbon, underscoring its agricultural significance. Building on this, the present work investigates its interaction with the insecticide fipronil to assess multifunctional applications, such as supporting controlled nutrient release while enhancing pesticide retention and thereby mitigating leaching and soil and water contamination.[4−7,24]

Received: July 7, 2025
Revised: September 24, 2025
Accepted: September 26, 2025
Published: October 6, 2025

Although HC exhibits promising properties, its low specific surface area necessitates activation to enhance porosity and eliminate organic matter and humic substances that may cause secondary pollution.[25−27] Activation can be achieved chemically, thermally, or thermochemically, generating materials with higher surface area and porosity,[28−31] commonly labeled activated hydrochar (AHC). In thermochemical activation, the precursor is mixed with an activating agent, such as KOH,[23] and subsequently treated thermally (400−1000 °C) under an inert or oxidizing atmosphere (e.g., N_2, CO_2). While physical activation avoids chemical residues, thermochemical activation is more efficient, operating at lower temperatures and shorter times, yielding larger pore volumes with reduced energy demand,[32] and potentially incorporating nutrients from the activating agent, which is advantageous for multifunctional use.

KOH thermochemical activation is widely employed for generating micro- and mesoporosity in carbon materials, thereby enhancing surface area and adsorption capacity, while remaining cost-effective compared to other activators.[32−35] KOH-to-precursor ratio and activation temperature are critical factors controlling the balance between pore formation and collapse.[31,35] Increased porosity promotes water retention, advantageous for soil applications, while nutrient incorporation, particularly potassium from KOH, can stimulate microbial activity and nutrient cycling.[36−38]

Several studies have demonstrated the capacity of activated carbonaceous materials to remove pesticides from environmental compartments, achieving removal efficiencies of 75−88%.[39−42] Nevertheless, research employing charcoal, biochar, HC, or activated carbons in pesticide adsorption remains limited.[41] Investigations such as the present study are therefore crucial to elucidate adsorption mechanisms under controlled conditions and to support future assessments involving environmental compartments and transport phenomena.[41,43]

In this study, sugar cane byproducts (bagasse and vinasse) underwent HTC in the presence of H_3PO_4, followed by KOH thermochemical activation to enhance pesticide adsorption, using fipronil as a model compound due to its extensive use in Brazil. Effects of activation parameters (HC:KOH ratios and activation temperatures) on HC composition, structure, morphology, textural properties, surface functional groups, and adsorption kinetics and mechanisms were systematically investigated. This work advances sustainable material development for environmental applications, supporting the transition to greener technologies and more sustainable agriculture.

2. MATERIALS AND METHODS

2.1. Materials and Chemicals. Biomass feedstocks for HC production (sugarcane bagasse and vinasse) were supplied by a sugarcane industry in São Paulo State, Brazil. Bagasse was registered in the National System for the Management of Genetic Heritage and Associated Traditional Knowledge (no. A0018C2), washed with distilled water, dried at 100 °C for 12 h, milled in a knife mill (Marconi, MA 340), sieved (<0.5 mm, Granutest), and stored at room temperature. Vinasse was collected in plastic containers, refrigerated at −4 °C, and thawed immediately prior to use. Reagent purity and fipronil stock solution details are provided in the Supporting Information (Section 1.1).

2.2. Preparation and KOH Thermochemical Activation of HC. HC was synthesized following patent WO2017132742A1,[44] using sugarcane bagasse and vinasse in a 1:20 (w:v) ratio with 4.0% H_3PO_4 (w:v) at 230 °C for 13 h. KOH activation was performed via wet impregnation:[23,35] 1.0 g of HC was mixed with 2.0 or 4.0 g of KOH dissolved in 10.0 mL of ultrapure water (HC:KOH, 1:2 or 1:4 w:w), stirred for 30 min (Fisatom, 752), dried at 105 °C for 14 h (Quimis, Q318M24), and thermally treated in a tubular furnace (EDG, FT-HI/20/Bipartite) at 500 °C or 700 °C for 1 h under N_2 (10 °C min^{-1}). After cooling, samples were washed with 0.5 mol L^{-1} HCl, rinsed to pH ∼7, dried at 100 °C for 24 h (Tecnik's, NL80/10CEL), ground, and sieved (0.15 mm, Bertel). AHC were labeled AHC-*x*−*y*, where *x* is activation temperature (5 = 500, 7 = 700 °C) and *y* is KOH ratio (2 = 1:2, 4 = 1:4).

2.3. Characterizations. Data characterization of HC employed in this study has been reported in previous works.[16−19] Due to the heterogeneous composition of the biomass used in the HTC process (sugarcane bagasse and vinasse), HC was resynthesized and re-characterized. AHCs were produced and characterized under these conditions for the first time, as detailed in Section 2.2.

Elemental composition (C, H, N) was determined using an elemental analyzer (Fisons, EA1108). Thermogravimetric analysis (TGA) was performed (Netzsch, STA 449 F3) from 30 °C to 700 °C under air at 10 °C min^{-1} (sample mass ≈10 mg). Functional groups were identified by Fourier-transform infrared spectroscopy (FTIR) (Bruker, Vertex70) with an attenuated total reflectance (ATR) accessory (PerkinElmer, SpectrumTwo), acquiring spectra in the 4000−400 cm^{-1} range at 2 cm^{-1} resolution with 128 scans in absorbance mode and then converted to transmittance. Inorganic phases were analyzed through powder X-ray diffraction (XRD; Rigaku, Miniflex 300) with Cu-Kα radiation (λ = 1.54 Å) at 10 mA and 30 kV, with steps of 0.02° s^{-1} in the 5−85° 2θ range, analyzed using X'Pert Highscore Plus software (Malvern Pananalytical) based on powder diffraction files from the International Centre for Diffraction Data (ICDD). Total metal in HC and AHC was quantified post-acid decomposition (method 3050B, EPA)[45] by flame atomic absorption spectrometry (FAAS) (Varian, AA240FS) in absorbance mode for magnesium, calcium, and iron, and emission mode for potassium.

Textural properties were assessed using N_2 adsorption−desorption isotherms (Quantachrome, Nova 1200). Specific surface area (S_{BET}) was calculated via the Brunauer, Emmett, and Teller (BET) method, pore volume and size via the Barrett, Joyner, and Halenda (BJH) method, and micropore volume via the Mikhail, Brunauer, Barrett, and Joyner (MP plot). Morphology was examined by scanning electron microscopy (SEM FEI, Quanta 250) coupled with Oxford X-MAX50 EDS for elemental mapping. Surface acidic groups (phenolic, lactone, and carboxyl) were quantified by Boehm titration.[46]

2.4. Adsorption Kinetics of Fipronil on HC and AHC. Fipronil adsorption on HC and AHCs (AHC-5-2, AHC-5-4, AHC-7-2, AHC-7-4) was performed in triplicate at 23 °C by adding 1.0 mg of each material (Shimadzu, AUW220D) to 200 mL of a 2 mg L^{-1} fipronil solution (dosage: 0.005 g L^{-1}), under constant orbital shaking (Solab, SL-180/DT) at 180 rpm for 0, 5, 15, 40, 60, 120, 300, 600, and 1440 min. This low concentration prevented fipronil precipitation due to its limited solubility. Aliquots were centrifuged at 3,400 rpm for 20 min (Novatecnica, NT-180) and filtered through a 0.45 μm nylon syringe filter (Filtrilo®, 13 mm).

Fipronil quantification was conducted using high-performance liquid chromatography with a diode array detector (HPLC-DAD; Agilent, 1220 Infinity) at 279 nm using OpenLab CDS Chemstation software, following a modified method.[47] Details are provided in Supplementary Data (Section 1.3). Chromatograms of the curves and analyses can be seen in Figures S1 and S2, respectively. The amount of fipronil adsorbed at time *t* (q_t, mg g^{-1}) was calculated by using eq 1. The removal efficiency, *E* (%), was calculated using eq 2.

$$q_t = \frac{(C_0 - C_t) \times V}{m} \tag{1}$$

$$E(\%) = \frac{(C_0 - C_t)}{C_0} \times 100 \tag{2}$$

where "C_0" and "C_t" denote the initial and at time "*t*" concentrations of the fipronil solution (mg L^{-1}), respectively, "*V*" represents the solution volume (L), and "*m*" is the mass of the adsorbent sample (g). The kinetic data of the fipronil adsorption experiment were evaluated

https://doi.org/10.1021/acssusresmgt.5c00321
ACS Sustainable Resour. Manage. 2025, 2, 1977−1985

according to pseudo-first order (PFO; eq S1), pseudo-second order (PSO; eq S2), intraparticle diffusion (ID; eq S3), and diffusion-chemisorption (DC; eq S4) nonlinear models.[48,49] To validate the model, the adjusted coefficient of determination "Adj. R^2" was calculated using eq S5, the root mean square error "RMSE" was calculated using eq S6, and the chi-squared (χ^2) was calculated using eq S7.[48]

3. RESULTS AND DISCUSSION

3.1. Characterization of HC and AHC. HC derived from the HTC of sugarcane bagasse with vinasse is a carbon-rich material, primarily composed of carbon (77.0%), nitrogen (2.8%), and hydrogen (2.4%) (Table 1). Thermochemical activation at 500 °C produced AHC-5-2 and AHC-5-4 with reduced carbon contents (52.3 and 56.5%, respectively). Activation at 700 °C yielded the lowest carbon content (34.4%) in AHC-7-2 (1:2 ratio) and the highest carbon content (67.6%) in AHC-7-4 (1:4 ratio). The marked carbon loss in AHC-7-2 results from KOH-induced gasification and redox reactions, releasing volatiles (CO_2, CO, CH_4) and forming potassium compounds (K_2CO_3, metallic K).[50,51] Conversely, the elevated carbon in AHC-7-4 is attributed to high-temperature KOH activation, which selectively removes oxygenated functional groups at higher KOH ratios, as described in eqs 3−6.[50]

Table 1. CHN Elemental Analysis and Mass Losses Obtained by TG Analysis for HC and AHC

	elemental analysis (%)			TG analysis (%)			
materials	C	H	N	1° stage	2° stage	3° stage	residue[a]
HC	77.0	2.4	2.8	3.1	5.7	73.5	16.2
AHC-5-2	52.3	2.2	1.9	14.0	68.4	—	6.3
AHC-5-4	56.5	2.2	1.5	18.8	60.4	—	13.8
AHC-7-2	34.4	2.4	1.2	26.2	57.5	—	10.7
AHC-7-4	67.6	2.2	2.9	19.1	42.5	—	34.4

[a]TGA residue in oxidant atmosphere; —: Not applied.

$$\mathrm{KOH} + (-\mathrm{COOH})/(-\mathrm{O}-\mathrm{C}{=}\mathrm{O}) \rightarrow \mathrm{K_2CO_3} + \mathrm{K} + \mathrm{H_2} + \mathrm{CO_2} \quad (3)$$

$$\mathrm{KOH} + (-\mathrm{C}{=}\mathrm{O})/(\mathrm{C}-\mathrm{O}-\mathrm{C}) \rightarrow \mathrm{K_2CO_3} + \mathrm{K} + \mathrm{H_2} + \mathrm{CO} \quad (4)$$

$$\mathrm{KOH} + (-\mathrm{O}-\mathrm{CH_3}) \rightarrow \mathrm{K_2CO_3} + \mathrm{K} + \mathrm{H_2} + \mathrm{CH_4} \quad (5)$$

$$\mathrm{KOH} + (\mathrm{C}-\mathrm{OH}) \rightarrow \mathrm{K_2CO_3} + \mathrm{K} + \mathrm{H_2O} + \mathrm{H_2} \quad (6)$$

The modification of the carbon composition by KOH is more pronounced at 700 °C, as molten KOH (360−380 °C) reacts with the carbonaceous matrix, promoting carbonyl decomposition and K_2CO_3 formation, leading to the release of K_2O and CO_2.[50,52] Nitrogen content decreased in AHC-5-2 (1.9 %), AHC-5-4 (1.5 %), and AHC-7-2 (1.2 %). Above 500 °C, amines can react with KOH to form nitrogen-containing aromatic species, such as pyridinic and pyrrolic groups,[53−55] which are more thermally stable and retained under prolonged KOH exposure, as observed in AHC-7-4, where nitrogen content remained constant (2.9 %).

The TG curve of the HC sample (Figure S3a) shows three mass-loss stages. The first (30−150 °C) corresponds to the removal of adsorbed water (Table 1). The second (200−300 °C) reflects the oxidation of labile carbon in O-alkyl groups and residual carbohydrates (cellulose/hemicellulose), consistent with the sugarcane bagasse precursor.[16,17] The third stage (350−650 °C) is attributed to the oxidation of more recalcitrant carbon, including lignin, aromatic structures, and polycondensed rings.[28,53,54] At 700 °C, 16.2% of the initial mass remains, indicating a significant inorganic fraction in the HC.

After thermochemical activation at 500 °C and 700 °C, all AHCs exhibited an increased mass loss between 30 °C and 150 °C (Table 1), indicating enhanced water affinity. The second stage (350−600 °C; Table 1) corresponded to the degradation of complex structures, aromatics, and polycondensed rings,[28,53,54] being more pronounced in the 1:2 activations. Consequently, materials activated at a 1:4 ratio retained more residue, reflecting a higher inorganic content, particularly, AHC-7-4 (34.4%; Table 1).

XRD analysis of HC (Figure S4) showed a broad, low-intensity halo between 5° and 35° (2θ), characteristic of an amorphous carbonaceous matrix.[56] Thermochemical activation altered the profiles, yielding two broad, low-intensity peaks: the first (002) arises from overlapping amorphous carbon halos due to cellulose and hemicellulose degradation,[57] while the second, centered at 43° (100), reflects planar aromatic layer formation from aromatic nuclei.[58]

Sharp, high-intensity peaks superimposed on the broad signal in HC (Figure S4) indicate crystalline inorganic phases. The peak at 20.9° (2θ) is assigned to SiO_2 (ICDD: 01-085-0457; hexagonal, P3221), commonly reported in HC from sugarcane bagasse and vinasse,[17,19] and attributed to sand residues on bagasse fibers or silicon in cell walls.[18,59] Anhydrite ($CaSO_4$, ICDD: 01-072-0916; orthorhombic, *Amma*) was also detected, with peaks at 25.4°, 30.9°, 39.7°, and 42.4° (2θ), likely formed by precipitation of SO_4^{2-} and Ca^{2+} ions abundant in vinasse.[60]

Additional peaks at 7.8°, 8.1°, and 27.5° (2θ) correspond to $Ca_3(PO_3)_6{\cdot}10H_2O$ (ICDD: 00-040-0008; *P*21/*n*), while those at 9.8°, 16.6°, 26.6°, 33.7°, and 36.6° (2θ) are assigned to $Ca_2P_6O_{17}$ (ICDD: 00-015-0203), and the peak at 17.4° is assigned to $Mg_3(PO_4)_2{\cdot}8H_2O$ (ICDD: 00-033-0877; *P*21/*m*). The formation of calcium and magnesium phosphates in HC from sugarcane bagasse and vinasse with H_3PO_4 as an additive has been documented.[17,18] Thus, Ca^{2+} and Mg^{2+} ions from vinasse likely precipitated with PO_4^{3-} from the additive and SO_4^{2-} from vinasse.

The limited number of peaks in the diffractograms hinders the precise identification of the AHC structural phases (Figure S4). This is likely due to the reaction of KOH during the thermochemical treatment with inorganic compounds in the HC, which removes them from the carbonaceous matrix, reducing the number of crystalline phases. Accordingly, total Mg, K, Fe, and Ca contents were quantified (Figure S5). HC exhibits elevated concentrations of K (2.9 mg g^{-1}), Fe (2.3 mg g^{-1}), Ca (3.2 mg g^{-1}), and Mg (20.0 mg g^{-1}) (Figure S5), reflecting their incorporation during HTC from vinasse, which contains K (3836 mg L^{-1}), Mg (491 mg L^{-1}), Fe (703 mg L^{-1}), and Ca (1070 mg L^{-1}).[61] Nevertheless, under acidic conditions, a fraction of these metals remains in the liquid phase.[19,60]

After thermochemical activation at 500 °C, Ca and Mg decreased 2.5- and 4.5-fold in a 1:2 ratio, whereas Fe and K increased 1.3- and 1.1-fold, respectively (Figure S5). Increasing

https://doi.org/10.1021/acssusresmgt.5c00321
ACS Sustainable Resour. Manage. 2025, 2, 1977−1985

the ratio to 1:4 reduced Mg 3.5-fold and Fe 1.1-fold, while Ca and K increased 1.2- and 5.9-fold, reflecting metal interactions with KOH and greater K incorporation. Similar trends were observed at 700 °C: at 1:2, Ca, Mg, and Fe decreased 2.7-, 9.3-, and 1.2-fold, respectively, and K increased 1.7-fold; at 1:4, Mg and Fe decreased 2.2- and 1.1-fold, whereas Ca and K increased 1.7- and 12.1-fold (Figure S5). The high K, Ca, and Mg content in AHC-7-4 correlates with the elevated residual mass determined by TGA (Table 1, 34.4 %).

Boehm titration of HC (Table S1) confirmed the presence of surface acid groups (3.64 mmol g^{-1}), predominantly phenolic (2.10 mmol g^{-1}). These findings are consistent with a previous study,[62] which quantified semi-volatile organic compounds in HC by gas chromatography and reported higher phenol content (6.0%) than fatty acids (4.9%) and ketones (0.3%). During HC production, hemicellulose and cellulose degrade thermally, whereas the more resistant lignin largely contributes to the material's phenolic character.[62,63]

After thermochemical activation at 500 °C and 700 °C with ratios of 1:2 and 1:4, the total acidic functional group content decreased, particularly at 700 °C and a 1:4 ratio, declining from 2.46 to 0.94 mmol g^{-1} (AHC-5-4 to AHC-7-4, Table S1). At elevated temperatures, KOH reacts with the carbon matrix, inducing decomposition that releases CO_2 and H_2O and promotes polycondensate formation. A comparable reduction in acidic groups was observed following KOH activation of sludge HC.[31]

FTIR analysis of HC (Figure 1a) exhibited a broad moderate-intensity band at 3255 cm^{-1}, characteristic of the

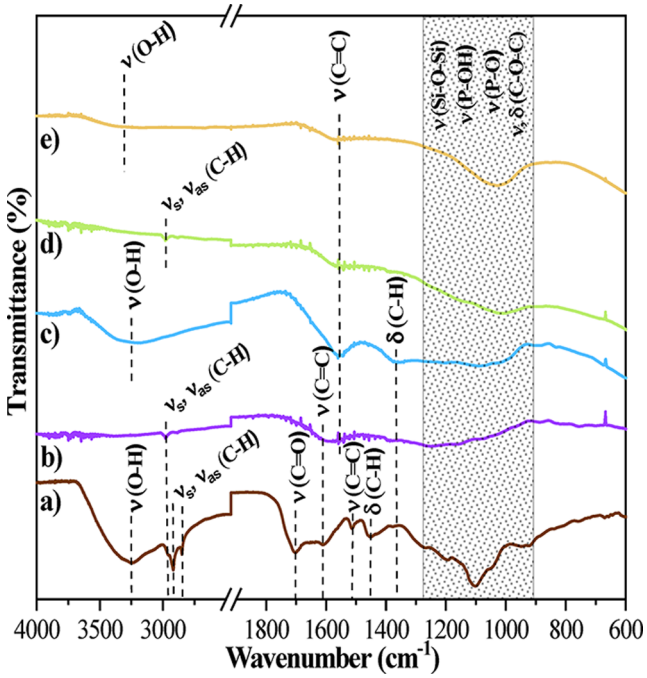

Figure 1. FTIR spectra obtained for (a) HC, (b) AHC-5-2, (c) AHC-5-4, (d) AHC-7-2, and (e) AHC-7-4.

O−H stretching of hydroxyl groups in the carbonaceous matrix. Low-intensity bands at 2958, 2923, and 2849 cm^{-1} corresponded to symmetric and asymmetric C−H stretching of methylene ($-CH_2$) and methyl ($-CH_3$) groups in aliphatic chains.[18,64,65] The band at 1704 cm^{-1} was assigned to C=O stretching in esters or carboxylic acids, while those at 1610 and 1510 cm^{-1} were attributed to C=C stretching and aromatic ring vibrations, reflecting the hydrophobic nature of HC.[18,64] Bands at 1451 and 1363 cm^{-1} were related to out-of-plane C−H vibrations in the aromatics. Overlapping bands between 1272 and 903 cm^{-1} were ascribed to C−O−C, P−O, and P−OH stretching, consistent with H_3PO_4 use in HTC, as well as Si−O−Si vibrations.[17] Silicon presence, reported in sugarcane bagasse, is linked to residual sand on bagasse fibers or silicon in cell walls.[18,59]

Following thermochemical activation at 500 °C and 700 °C, FTIR spectra revealed pronounced alterations in the surface chemistry compared to the initial HC (Figure 1b−e). For AHC-5-2 (Figure 1b), only bands at 2958, 1610, 1555, 1363 cm^{-1} and 1272−903 cm^{-1} remained, corresponding to C−H, C=C, C−H, Si−O−Si, P−O−H, P−O, and C−O−C bonds, with all other HC bands eliminated (Figure 1a). In the 1:4 ratio (Figure 1c), a similar profile was observed, except for the disappearance of the 2958 cm^{-1} C−H band and the appearance of a broad, low-intensity O−H band, likely due to the higher KOH content. KOH reacts with stable carbon fragments, creating vacancies subsequently occupied by OH^-, thereby introducing oxygen.[50]

Activation at 700 °C with a 1:2 ratio (Figure 1d) yielded a spectrum similar to that at 500 °C (Figure 1b), but with the disappearance of the 1610 and 1363 cm^{-1} bands assigned to C=C and C−H bonds, respectively. At a 1:4 ratio (Figure 1e), the spectrum resembled that at 500 °C (Figure 1c), with loss of the 2958 cm^{-1} band (C−H) and appearance of the 3255 cm^{-1} band (O−H). These shifts indicate significant surface modification of the HC, reflecting functional group removal and formation driven by elevated temperature and KOH−carbon interactions.[23]

Morphological analysis of HC (Figure 2a−o) revealed spherical particles (3−4 μm) and irregular agglomerates, including rod-like (~10 μm) and platelike structures (Figure 2a,b). Carbonaceous spheres originate from complete hemicellulose decomposition and partial cellulose degradation via hydrolysis and polymerization,[58] a process enhanced by the high temperatures and acidic conditions of HTC.[17,66,67] The irregular agglomerates likely arise from partially degraded cellulose, residual lignin,[58] and inorganic compounds such as calcium and magnesium sulfates and phosphates (Figure S5). HC exhibits brighter regions in the BSE-mode image, indicating the presence of these metals (Figure 2c).

Thermochemical activation at 500 °C (Figure 2d,e) and 700 °C (Figure 2j,k) with a 1:2 KOH ratio produced microparticles with abundant cavities, a hallmark of KOH-activated carbonaceous materials exhibiting well-developed porosity and high surface area.[57,66] Materials activated at 700 °C (Figure 2j,k,m,n) showed more pronounced cavities than those at 500 °C (Figure 2d,e,g,h), reflecting greater degradation of the carbon matrix. Metal quantification (Figure S5) has shown that increasing the KOH ratio during thermochemical activation resulted in higher K incorporation into the material. This is evident in BSE-mode SEM images, where brighter regions appear in Figure 2f,i,l,o. In AHC-7-4 (Figure 2o), the material with the highest K content, cubic-shaped structures characteristic of inorganic phases, is more prominent.

HC exhibited a type III reversible N_2 adsorption−desorption isotherm (Figure S6a), characteristic of non-porous or macroporous materials,[67,68] with low specific surface area (33 m^2 g^{-1}) and pore volume (0.09 cm^3 g^{-1}) (Table 2), in agreement with HCs derived from sucrose and orange

https://doi.org/10.1021/acssusresmgt.5c00321
ACS Sustainable Resour. Manage. 2025, 2, 1977−1985

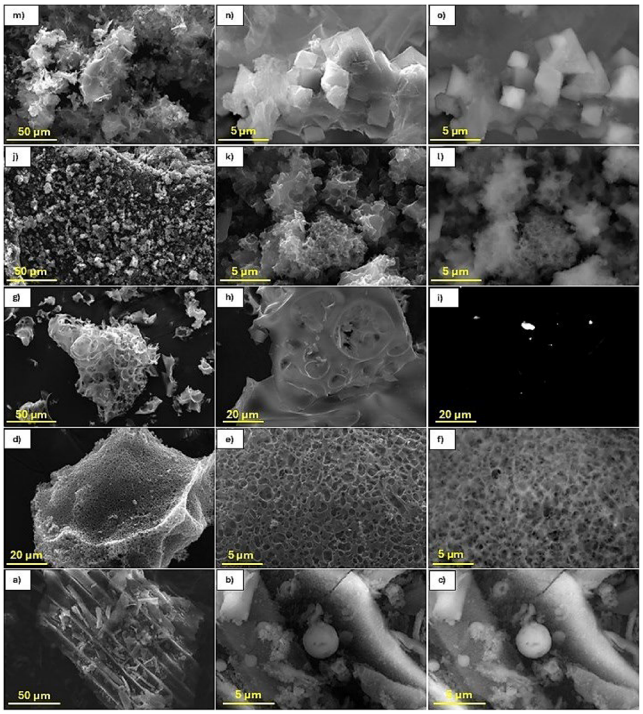

Figure 2. SEM images of HC (a, b), AHC-5-2 (d, e), AHC-5-7 (g, h), AHC-7-2 (j, k), AHC-7-4 (m, n), and BSE images of HC (c), AHC-5-2 (f), AHC-5-4 (i), AHC-7-2 (l), and AHC-7-4(o).

Table 2. Specific Surface Area, Pore Volume, and Average Pore Diameter Obtained from N_2 Adsorption−Desorption Isotherms for HC and AHCs

parameters	HC	AHC-5-2	AHC-5-4	AHC-7-2	AHC-7-4
S_{BET} (m^2 g^{-1})[a]	33	261	333	620	870
average pore diameter (nm)	11.5	1.4	3.7	1.2	3.3
total pore volume (cm^3 g^{-1})	0.09	0.19	0.31	0.38	0.72
mesopore volume (cm^3 g^{-1})[b]	—	0.05	0.14	0.07	0.21
micropore volume (cm^3 g^{-1})[c]	—	0.14	0.17	0.31	0.51

[a]Determined using the BET method. [b]Determined using the BJH method. [c]Determined using MP plot method; —: Not applied.

peel.[35,58,69] Thermochemical activation at 500 °C and 700 °C converted the isotherm to type *I*(*b*),[67,68] reflecting a broader distribution of wider micropores and narrower mesopores (Figure S6b,c), consistent with increased surface area and pore volume, particularly for AHC-7-4 (870 and 0.72 cm^3 g^{-1}, Table 2). Overall, AHC displayed a micropore-dominant structure (0.14−0.51 cm^3 g^{-1}) with a significant mesopore contribution (0.05−0.21 cm^3 g^{-1}).

Increasing the activation temperature from 500 °C to 700 °C predominantly enhanced micropore formation (by factors of 2.2−3) relative to mesopores (by factors of 1.4−1.5), resulting in AHCs with higher micropore content at 700 °C (71−82%) than at 500 °C (55−74%), consistent with previous reports.[70] Moreover, higher KOH:HC ratios increased the average pore diameter (1.2−1.4 to 3.3−3.7 nm), irrespective of temperature, converting micropores into mesopores and raising the mesopore fraction (18−26% to 29−45%), in agreement with the literature.[56,71]

3.2. Fipronil Adsorption. Fipronil adsorption increased sharply within the first 15 min (Figure 3a), reaching 106, 131,

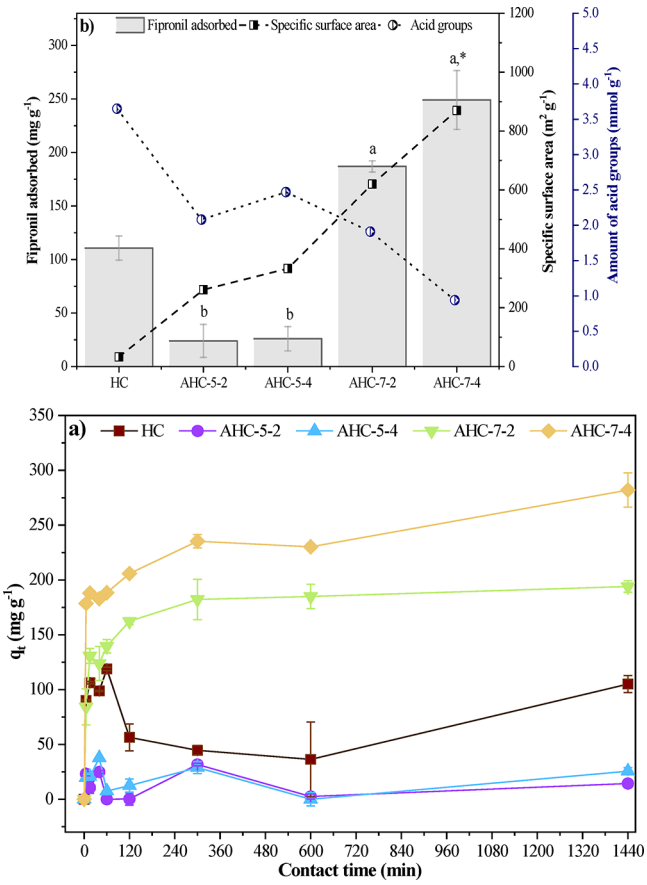

Figure 3. (a) Kinetic profile of fipronil adsorption by HC before and after thermochemical activation (AHC-5-2, AHC-5-4, AHC-7-2, and AHC-7-4); and (b) amount of fipronil adsorbed in 1440 min using HC and AHC and its relationship with the specific surface area and the amount of acid groups in these materials. [a] Statistically significant positive difference about HC; [b] Statistically significant negative difference about HC; * Statistically significant difference between all treatments.

and 188 mg g^{-1} for HC, AHC-7-2, and AHC-7-4, respectively. In contrast, AHC-5-2 and AHC-5-4 exhibited capacities 12- and 9-fold lower, at 11 and 21 mg g^{-1}, respectively. Between 15 and 600 min, HC, AHC-5-2, and AHC-5-4 showed a temporary decline in adsorption, reflecting dynamic equilibrium, with rapid initial saturation followed by partial desorption, before stabilizing. HC and 500 °C AHCs reached near-equilibrium after 300 min, whereas AHC-7-2 and AHC-7-4 continued to increase, with AHC-7-4 displaying a persistent upward trend. Final adsorption capacities were 110, 24, 26, 187, and 249 mg g^{-1} for HC, AHC-5-2, AHC-5-4, AHC-7-2, and AHC-7-4, corresponding to removal efficiencies of 26, 7, 6, 54, and 61%, respectively. The moderate efficiencies can be attributed to the low adsorbent dose (0.005 g L^{-1}), limited fipronil solubility, heterogeneous surface chemistry of the precursors, and steric hindrance effects.

HC is a non-porous material with low specific surface area (S_{BET}: 33 m^2 g^{-1}, Table 2), removing 110 mg g^{-1} of fipronil over 1440 min (Figure 3b). Boehm titration (Table S1) revealed ∼3.64 mmol g^{-1} of acidic surface groups, which, according to Lewis theory, can interact with electron-donating

https://doi.org/10.1021/acssusresmgt.5c00321
ACS Sustainable Resour. Manage. 2025, 2, 1977−1985

moieties such as amines, imines, and sulfonyls in fipronil. Aromatic domains may also interact with the π-electron systems of the benzene and imidazole rings, further contributing to adsorption.[14,69]

Thermochemical activation at 500 °C with ratios of 1:2 and 1:4 produced the lowest adsorption capacities (AHC-5-2:24 mg g^{-1}; AHC-5-4:26 mg g^{-1}, Figure 3b), whereas activation at 700 °C yielded the highest (AHC-7-2:187 mg g^{-1}; AHC-7-4:249 mg g^{-1}, Figure 3b). One-way ANOVA confirmed these differences were significant relative to HC ($p < 0.01$). Increasing the activation temperature altered the carbonaceous matrix, reducing polar functionalities while enhancing specific surface area (Tables S1 and S2). At 500 °C, the loss of acidic groups outweighed the modest surface gain, limiting fipronil adsorption to polar interactions. In contrast, at 700 °C, extensive pore development and higher surface area promoted non-polar interactions, particularly with aromatic domains, as the dominant adsorption mechanism. Kinetic modeling (PFO, PSO, ID, DC) was applied to identify the best fit to the experimental data (Table S2 and Figure S7).

The PFO and DC models best fitted the fipronil adsorption data for HC, AHC-5-2, and AHC-5-4 (Table S2), indicating simultaneous physical, chemical, and diffusion-controlled processes.[48,72] This accounts for the negative fluctuations in their kinetics (Figure 3a), reflecting the dynamic equilibrium characteristic of physical interactions. In contrast, PSO and DC models described adsorption by AHC-7-2 and AHC-7-4 (Table S2), where chemical interactions and diffusion predominated, explaining the kinetic plateau (Figure 3a) due to largely irreversible chemical binding. Precise mechanistic differentiation remains challenging owing to material heterogeneity. The higher capacity of HC compared to AHC-5-2 and AHC-5-4 was ascribed to its greater surface concentration of acidic functional groups (3.64 vs 2.08 and 2.46 mmol g^{-1}, Table S1), dominated by phenolic moieties. Conversely, AHC-7-2 and AHC-7-4 exhibited the highest capacities, reflecting their larger specific surface areas (620 and 870 m^2 g^{-1}) and micropore volumes (0.31 and 0.51 cm^3 g^{-1}, Table 2).

Although increasing the KOH:biomass ratio from 1:2 to 1:4 at 500 °C led to a slight increase in surface area (from 261 to 333 m^2 g^{-1}; Table 2) and acid group content (from 2.08 to 2.46 mmol g^{-1}; Table S1), this had no significant effect on fipronil removal. On the other hand, at 700 °C, increasing the KOH dosage significantly improved fipronil adsorption, which was associated with substantial increases in specific surface area (from 620 to 870 m^2 g^{-1}; Table 2) and average pore diameter (from 1.2 to 3.3 nm; Table 2), despite a 50% reduction in acid functional groups, mainly carboxylic groups (from 1.61 to 0.47 mmol g^{-1}; Table S1). Attempts to obtain fipronil adsorption isotherms were hampered by its low solubility in water, which led to precipitation at higher concentrations; therefore, only kinetic studies were carried out.

HC thermochemically activated with KOH at 700 °C demonstrated superior fipronil removal, both in capacity and kinetic stability, highlighting the critical role of an increased specific surface area. Thermochemical activation effectively modified the HC structure, enhancing its suitability for pesticide adsorption. AHC-7-4 exhibited the highest adsorption capacity in this study, exceeding most reported materials (Table 3) and only being surpassed by a modified zeolite,[73] which required an 800-fold higher dosage (4.0 vs 0.005 g L^{-1}), emphasizing the high efficiency of AHC-7-4.

Table 3. Comparison of the Maximum Adsorption Capacity of Fipronil Adsorbed by AHC at 700 °C in a 1:4 Ratio with Other Materials Described in the Literature

materials	q (mg g^{-1})	refs
AHC-7-4	249	this study
metal−organic framework M-ZIF-8@ZIF-67	3.9	8
Ce_{25}ZSM-5 modified zeolite	598.8	73
Microplastic particles (PBS)	0.2	74
magnetic composite hydrogel Fe_3O_4/SiO_2/PDEAEMA/CS	82.5	75

4. CONCLUSIONS

Thermochemical activation of HC derived from sugarcane by-products effectively modulated its physicochemical and textural properties, yielding pronounced differences in fipronil adsorption. Activation at 500 °C reduced the adsorption capacity relative to HC, reflecting the loss of aromatic and acidic functional groups. Conversely, activation at 700 °C, particularly with a 1:4 KOH ratio, markedly increased surface area and microporosity, resulting in adsorption capacities up to 249 mg g^{-1}. This shift indicates a change in adsorption mechanism from interactions dominated by functional groups in HC to chemical and diffusion-controlled processes in activated carbons with high specific surface areas (up to 870 m^2 g^{-1}). These findings demonstrate that KOH activation is a viable strategy to engineer multifunctional carbonaceous materials from agro-industrial residues for pesticide mitigation, supporting circular economy and sustainability objectives. Given the modest removal efficiencies (~61%), future work should investigate more soluble pesticides, higher adsorbent dosages, alternative activating agents, and soil-based assessments of material-pesticide interactions to enhance performance and environmental applicability.

■ ASSOCIATED CONTENT

Data Availability Statement

The raw data are available at https://repositorio.unesp.br/items/e92a2c23-3758-4ba0-ba12-2a4989b603d3.

Supporting Information

The Supporting Information is available free of charge at https://pubs.acs.org/doi/10.1021/acssusresmgt.5c00321.

Reagent purity; kinetic model equations (PFO, PSO, ID, DC); error functions (Adj. R^2, RMSE, χ^2); FAAS metal quantification; oxygenated functional group table; chromatograms and fipronil removal analyses; TG/DTG curves; XRD diffractograms; FAAS figures; N_2 adsorption−desorption isotherms; nonlinear kinetic model applications (PDF)

■ AUTHOR INFORMATION

Corresponding Author

Márcia C. Bisinoti − *Institute of Biosciences, Modern Languages and Exact Sciences (IBILCE), Department of Chemistry and Environmental Sciences (DQCA), Laboratory of Environmental Sciences Studies (LECA), São Paulo State University (UNESP), São José do Rio Preto, São Paulo 15054-000, Brazil;* orcid.org/0000-0002-4631-2400; Email: marcia.bisinoti@unesp.br

https://doi.org/10.1021/acssusresmgt.5c00321
ACS Sustainable Resour. Manage. 2025, 2, 1977−1985

Authors

Gabriela A. Nogueira − *Institute of Biosciences, Modern Languages and Exact Sciences (IBILCE), Department of Chemistry and Environmental Sciences (DQCA), Laboratory of Environmental Sciences Studies (LECA), São Paulo State University (UNESP), São José do Rio Preto, São Paulo 15054-000, Brazil;* orcid.org/0000-0002-0878-6162

Márcio J. Laranja − *Institute of Biosciences, Modern Languages and Exact Sciences (IBILCE), Department of Chemistry and Environmental Sciences (DQCA), Laboratory of Environmental Sciences Studies (LECA), São Paulo State University (UNESP), São José do Rio Preto, São Paulo 15054-000, Brazil*

Suelen A. Mondek − *Institute of Biosciences, Modern Languages and Exact Sciences (IBILCE), Department of Chemistry and Environmental Sciences (DQCA), Laboratory of Environmental Sciences Studies (LECA), São Paulo State University (UNESP), São José do Rio Preto, São Paulo 15054-000, Brazil*

Laís H. S. Vieira − *Department of Physical, Science Centre, Federal University of Ceará, Fortaleza, Ceará 60440-900, Brazil;* orcid.org/0000-0002-1204-2510

Mauricio Boscolo − *Institute for Bioenergy Research (IPBen-UNESP), São José do Rio Preto, São Paulo 15054-000, Brazil*

Odair P. Ferreira − *Advanced Functional Materials Laboratory (LaMFA), Department of Chemistry, State University of Londrina (UEL), Londrina, Paraná 86055-900, Brazil*

Altair B. Moreira − *Institute of Biosciences, Modern Languages and Exact Sciences (IBILCE), Department of Chemistry and Environmental Sciences (DQCA), Laboratory of Environmental Sciences Studies (LECA), São Paulo State University (UNESP), São José do Rio Preto, São Paulo 15054-000, Brazil;* orcid.org/0000-0001-7903-2360

Complete contact information is available at: https://pubs.acs.org/10.1021/acssusresmgt.5c00321

Author Contributions

G.A.N.: writing-original draft, review, and editing; methodology; investigation; conceptualization; data curation. M.J.L.: writing-original draft, review, and editing; methodology; investigation; conceptualization; data curation. S.A.M.: writing-review and editing; data curation. L.H.S.V.: methodology; writing-review and editing. M.B.: methodology, writing-review and editing. O.P.F.: writing-review and editing; methodology; investigation; conceptualization; data curation. A.B.M.: writing-review; resources; investigation. M.C.B.: writing-review and editing; resources; supervision; investigation; conceptualization; data curation. G.A.N. and M.J.L.: equal contribution.

Funding

G.A.N. acknowledges support from the CAPES-DS scholarship (Process 88887.843931/2023-00). M.J.L. and S.A.M. received CAPES-DS scholarships (Processes 88882.434479/2019-01 and 88887.606590/2021-00, respectively). M.C.B. was supported by CNPq (Grants 445487/2014-3 and 303232/2022-6) and FAPESP (Grants 2018/15733-7, 2020/02471-4, 2021/09126-3; 2024/17456-1). A.B.M. acknowledges FAPESP support (Grants 2014/17511-0 and 2017/26718-6). O.P.F. was supported by FUNCAP (PRONEX PR2-0101-00006.01.00/15) and CNPq (Grants 409205/2023-0 and 310821/2022-3).

Funding

The Article Processing Charge for the publication of this research was funded by the Coordenacao de Aperfeicoamento de Pessoal de Nivel Superior (CAPES), Brazil (ROR identifier: 00x0ma614).

Notes

The authors declare no competing financial interest.

■ ACKNOWLEDGMENTS

We acknowledge support from the CAPES scholarships, CNPq, FAPESP, and FUNCAP project funding. The authors thank IPBen for assistance with FTIR (FAPESP, grant 2017/13230-5), XRD, TGA, and HPLC-DAD analyses.

■ REFERENCES

(1) Steffen, W.; Richardson, K.; Rockström, J.; Cornell, S. E.; Fetzer, I.; Bennett, E. M.; Biggs, R.; Carpenter, S. R.; De Vries, W.; De Wit, C. A.; Folke, C.; Gerten, D.; Heinke, J.; Mace, G. M.; Persson, L. M.; Ramanathan, V.; Reyers, B.; Sörlin, S. Planetary Boundaries: Guiding Human Development on a Changing Planet. *Science* **2015**, *347*, 347.

(2) Molotoks, A.; Stehfest, E.; Doelman, J.; Albanito, F.; Fitton, N.; Dawson, T. P.; Smith, P. Global Projections of Future Cropland Expansion to 2050 and Direct Impacts on Biodiversity and Carbon Storage. *Glob Chang Biol.* **2018**, *24* (12), 5895−5908.

(3) Moreira, R. A.; González, M. P.; Dias, M. A.; Ogura, A. P.; Mena, F.; Montagner, C. C.; Espíndola, E. L. G.; Blasco, J.; Parra, G.; Araújo, C. V. M. Ecological Consequences When Organisms Avoid a Contaminated Environment: A Study Evaluating the Toxicity of Fipronil. *Sci. Total Environ.* **2024**, *926*, No. 171480.

(4) Granetto, M.; Bianco, C.; Tosco, T. The Role of Soil Amendments in Limiting the Leaching of Agrochemicals: Laboratory Assessment for Copper Sulphate and Dicamba. *J. Clean. Prod.* **2024**, *474*, No. 143532.

(5) Mamboungou, J.; Fernandes, É. K. K.; Vieira, L. G.; Rocha, T. L. Hazardous Fipronil Insecticide Effects on Aquatic Animals Health: Historical Review and Trends. *Science of the Total Environment* **2024**, *954*, No. 176334. Elsevier B.V. December 1

(6) Abraham, J.; Gajendiran, A. Biodegradation of Fipronil and Its Metabolite Fipronil Sulfone by Streptomyces Rochei Strain AJAG7 and Its Use in Bioremediation of Contaminated Soil. *Pestic Biochem Physiol* **2019**, *155*, 90−100.

(7) Triques, M. C.; Oliveira, D.; Goulart, B. V.; Montagner, C. C.; Espíndola, E. L. G.; de Menezes-Oliveira, V. B. Assessing Single Effects of Sugarcane Pesticides Fipronil and 2,4-D on Plants and Soil Organisms. *Ecotoxicol. Environ. Saf.* **2021**, *208*, No. 111622.

(8) Liu, F.; Li, H.; Zhang, X.; Hu, H.; Yuan, B.; You, J. Quantitative Differentiation of Toxicity Contributions and Predicted Global Risk of Fipronil and Its Transformation Products to Aquatic Invertebrates. *Water Res.* **2024**, *255*, No. 121461.

(9) Bhatt, P.; Gangola, S.; Ramola, S.; Bilal, M.; Bhatt, K.; Huang, Y.; Zhou, Z.; Chen, S. Insights into the Toxicity and Biodegradation of Fipronil in Contaminated Environment. *Microbiol. Res.* **2023**, *266*, No. 127247.

(10) Pisa, L. W.; Amaral-Rogers, V.; Belzunces, L. P.; Bonmatin, J. M.; Downs, C. A.; Goulson, D.; Kreutzweiser, D. P.; Krupke, C.; Liess, M.; Mcfield, M.; Morrissey, C. A.; Noome, D. A.; Settele, J.; Simon-Delso, N.; Stark, J. D.; Van Der Sluijs, J. P.; Van Dyck, H.; Wiemers, M. Effects of Neonicotinoids and Fipronil on Non-Target Invertebrates. *Environmental Science and Pollution Research* **2015**, *22* (1), 68−102.

(11) Silva, L. C. M.; Moreira, R. A.; Pinto, T. J. S.; Ogura, A. P.; Yoshii, M. P. C.; Lopes, L. F. P.; Montagner, C. C.; Goulart, B. V.; Daam, M. A.; Espíndola, E. L. G. Acute and Chronic Toxicity of 2,4-D and Fipronil Formulations (Individually and in Mixture) to the Neotropical Cladoceran Ceriodaphnia Silvestrii. *Ecotoxicology* **2020**, *29* (9), 1462−1475.

(12) Bose, S.; Senthil Kumar, P.; Rangasamy, G.; Prasannamedha, G.; Kanmani, S. A Review on the Applicability of Adsorption Techniques for Remediation of Recalcitrant Pesticides. *Chemosphere* **2023**, *313*, No. 137481.
(13) Heryanto, H.; Tahir, D.; Abdullah, B.; Kavgaci, M.; Rinovian, A.; Masrour, R.; Prasad, V. S. R.; Sayyed, M. I. Carbon as a Multifunctional Material in Supporting Adsorption Performance for Water Treatment: Science Mapping and Review. *Desalination and Water Treatment* **2024**, *320*, No. 100758. Elsevier B.V. October 1
(14) Liu, H.; Long, J.; Zhang, K.; Li, M.; Zhao, D.; Song, D.; Zhang, W. Agricultural Biomass/Waste-Based Materials Could Be a Potential Adsorption-Type Remediation Contributor to Environmental Pollution Induced by Pesticides-A Critical Review. *Science of the Total Environment* **2024**, *946*, No. 174180. Elsevier B.V. October 10,
(15) Gong, M.; Xu, F.; Liu, P.; Xu, Q.; Su, Y.; Fan, Y.; Li, M. A Review of Biomass Hydrochar as an Adsorbent: Performance, Modification, and Applications. *Journal of Water Process Engineering* **2025**, *71* (71), No. 107314.
(16) Bento, L. R.; Castro, A. J. R.; Moreira, A. B.; Ferreira, O. P.; Bisinoti, M. C.; Melo, C. A. Release of Nutrients and Organic Carbon in Different Soil Types from Hydrochar Obtained Using Sugarcane Bagasse and Vinasse. *Geoderma* **2019**, *334*, 24−32.
(17) Melo, C. A.; Junior, F. H. S.; Bisinoti, M. C.; Moreira, A. B.; Ferreira, O. P. Transforming Sugarcane Bagasse and Vinasse Wastes into Hydrochar in the Presence of Phosphoric Acid: An Evaluation of Nutrient Contents and Structural Properties. *Waste Biomass Valorization* **2017**, *8* (4), 1139−1151.
(18) Bento, L. R.; Spaccini, R.; Cangemi, S.; Mazzei, P.; de Freitas, B. B.; de Souza, A. E. O.; Moreira, A. B.; Ferreira, O. P.; Piccolo, A.; Bisinoti, M. C. Hydrochar Obtained with By-Products from the Sugarcane Industry: Molecular Features and Effects of Extracts on Maize Seed Germination. *J. Environ. Manage.* **2021**, *281*, No. 111878.
(19) Silva, C. C.; Melo, C. A.; Soares Junior, F. H.; Moreira, A. B.; Ferreira, O. P.; Bisinoti, M. C. Effect of the Reaction Medium on the Immobilization of Nutrients in hydrochars Obtained Using Sugarcane Industry Residues. *Bioresour Technol.* **2017**, *237*, 213−221.
(20) dos Santos, J. V.; Fregolente, L. G.; Moreira, A. B.; Ferreira, O. P.; Mounier, S.; Viguier, B.; Hajjoul, H.; Bisinoti, M. C. Humic-like Acids from hydrochars: Study of the Metal Complexation Properties Compared with Humic Acids from Anthropogenic Soils Using PARAFAC and Time-Resolved Fluorescence. *Sci. Total Environ.* **2020**, *722*, No. 137815.
(21) Kambo, H. S.; Dutta, A. A Comparative Review of Biochar and Hydrochar in Terms of Production, Physico-Chemical Properties and Applications. *Renewable and Sustainable Energy Reviews. Elsevier Ltd* **2015**, *45*, 359−378.
(22) Funke, A.; Ziegler, F. Hydrothermal Carbonization of Biomass: A Summary and Discussion of Chemical Mechanisms for Process Engineering. *Biofuels, Bioproducts and Biorefining.* **2010**, *4*, 160−177. March
(23) Nogueira, G. A.; Fregolente, L. G.; Pereira, L. S.; Laranja, M. J.; Moreira, A. B.; Ferreira, O. P.; Bisinoti, M. C. Magnetic Activated Carbonaceous Materials from Sugarcane Bagasse: Preparation, Characterization, and Hexavalent Chromium Removal. *Materials Today Sustainability* **2024**, *28* (28), No. 101040.
(24) Li, T.; Lu, M.; Gao, Y.; Huang, X.; Liu, G.; Xu, D. Double Layer MOFs M-ZIF-8@ZIF-67: The Adsorption Capacity and Removal Mechanism of Fipronil and Its Metabolites from Environmental Water and Cucumber Samples. *J. Adv. Res.* **2020**, *24*, 159−166.
(25) Shi, Y.; Li, H.; Rong, Y.; Bai, L.; Chi, M.; Xu, X.; Li, C.; Bai, H.; Liu, Y. The Improving of Cd2+ Adsorption Performance of Hydrochar Obtained from Corn Straw Waste with KOH Activation. *Water Air Soil Pollut* **2022**, *233*, 12.
(26) De Smedt, J.; Arauzo, P. J.; Ronsse, F. Molten Salts vs Conventional Activating Agents for Activated Carbon Production: A Comprehensive Review. *J. Anal Appl. Pyrolysis* **2025**, *192*, No. 107239.
(27) Chebil, A.; El Golli, A.; Achour, B.; Messaoud, N. B.; Lufrano, F. Towards a Sustainable Future: Advances and Roadmap of Activated Carbon as a Cost-Effective Bio-Nanomaterial for Electrochemical Devices: An up-to-Date Review. *Sustainable Mater. Technol.* **2025**, No. e01603.
(28) El-Sayed, G. O.; Yehia, M. M.; Asaad, A. A. Assessment of Activated Carbon Prepared from Corncob by Chemical Activation with Phosphoric Acid. *Water Resour Ind.* **2014**, *7*−*8*, 66−75.
(29) Fang, J.; Gao, B.; Zimmerman, A. R.; Ro, K. S.; Chen, J. Physically (CO2) Activated hydrochars from Hickory and Peanut Hull: Preparation, Characterization, and Sorption of Methylene Blue, Lead, Copper, and Cadmium. *RSC Adv.* **2016**, *6* (30), 24906−24911.
(30) González-García, P. Activated Carbon from Lignocellulosics Precursors: A Review of the Synthesis Methods. Characterization Techniques and Applications. *Renewable Sustainable Energy Rev.* **2018**, *1*, 1393−1414.
(31) Khoshbouy, R.; Takahashi, F.; Yoshikawa, K. Preparation of High Surface Area Sludge-Based Activated Hydrochar via Hydrothermal Carbonization and Application in the Removal of Basic Dye. *Environ. Res.* **2019**, *175*, 457−467. (April)
(32) Suhas; Gupta, V. K.; Carrott, P. J. M.; Singh, R.; Chaudhary, M.; Kushwaha, S. Cellulose: A Review as Natural, Modified and Activated Carbon Adsorbent. *Bioresource Technology* **2016**, *216*, 1066−1076. Elsevier Ltd September 1
(33) Sultana, A. I.; Reza, M. T. Investigation of Hydrothermal Carbonization and Chemical Activation Process Conditions on Hydrogen Storage in Loblolly Pine-Derived Superactivated hydrochars. *Int. J. Hydrogen Energy* **2022**, *47* (62), 26422−26434.
(34) Wang, J.; Chen, S.; Xu, J. Y.; Liu, L. C.; Zhou, J. C.; Cai, J. J. High-Surface-Area Porous Carbons Produced by the Mild KOH Activation of a Chitosan Hydrochar and Their CO2 Capture. *Xinxing Tan Cailiao/New Carbon Materials* **2021**, *36* (6), 1081−1093.
(35) Vieira, L. H. S.; Sganzerla Sabino, C. M.; Soares Júnior, F. H.; Rocha, J. S.; Castro, M. O.; Alencar, R. S.; Souza da Costa, L.; Viana, B. C.; Jardim de Paula, A.; Soares, J. M.; Gomes Souza Filho, A.; Otubo, L.; Fechine, P. B. A.; Ghosh, A.; Ferreira, O. P. Strategic Design of Magnetic Carbonaceous Nanocomposites and Its Application as Multifunctional Adsorbent. *Carbon N Y* **2020**, *161*, 758−771.
(36) Zhang, M. S.; Chiu, C. F.; Zhou, Y. Z.; Wang, Y. N. Compression and Water Retention Behavior of Saline Soil Improved by MICP Combined with Activated Carbon. *Sci. Rep* **2024**, *14* (1), 14.
(37) Brtnicky, M.; Mustafa, A.; Hammerschmiedt, T.; Kintl, A.; Trakal, L.; Beesley, L.; Ryant, P.; Omara-Ojungu, C.; Baltazar, T.; Holatko, J. Pre-Activated Biochar by Fertilizers Mitigates Nutrient Leaching and Stimulates Soil Microbial Activity. *Chemical and Biological Technologies in Agriculture* **2023**, *10*, 1.
(38) Khati, P.; Mishra, P.; Parihar, M.; Kumari, A.; Joshi, S.; Bisht, J.; Pattanayak, A. Potassium Solubilization and Mobilization: Functional Impact on Plant Growth for Sustainable Agriculture. In *Advances in Plant Microbiome and Sustainable Agriculture: Functional Annotation and Future Challenges*; Springer Singapore: Singapore, 2020; pp 21−39.
(39) Motúzová, T.; Koutník, I.; Vráblová, M. Removal of Pesticides from Water by Adsorption on Activated Carbon Prepared from Invasive Plants. *Water Air Soil Pollut* **2024**, *235*, 12.
(40) Patra, S.; Das, D.; Singh, M.; Gupta, S. Potato Peel Biochar: A Sustainable Material for the Removal of Pesticides and Soil Amendment for Crop Productivity. *Ann. Plant Soil Res.* **2024**, *26*, 578−584.
(41) Holanda, M. A. S.; Coelho Menezes, J. M.; Coutinho, H. D. M.; Teixeira, R. N. P. Effectiveness of Biochar as an Adsorbent for Pesticides: Systematic Review and Meta-Analysis. *J. Environ. Manage* **2023**, *345*, No. 118719.
(42) Spaltro, A.; Pila, M.; Simonetti, S.; Álvarez-Torrellas, S.; Rodríguez, J. G.; Ruiz, D.; Compañy, A. D.; Juan, A.; Allegretti, P. Adsorption and Removal of Phenoxy Acetic Herbicides from Water

by Using Commercial Activated Carbons: Experimental and Computational Studies. *J. Contam Hydrol* **2018**, *218*, 84−93.
(43) Yan, J.; Quan, G. Sorption Behavior of Dimethyl Phthalate in Biochar-Soil Composites: Implications for the Transport of Phthalate Esters in Long-Term Biochar Amended Soils. *Ecotoxicol. Environ. Saf.* **2020**, *205*, No. 111169.
(44) Melo, C. A.; Bisinoti, M. C.; Ferreira, O. P.; Moreira, A. B.; Santana, R. L.; Soares Júnior, F. H. Method for Producing Organo-Mineral Fertilizer by Hydrothermal Carbonization of Sugarcane Vinasse and Bagasse and Thus Obtained Product. WO2017132742A1, 2017.
(45) Environmental Protection Agency, U. *Method 3050B Acid Digestion of Sediments, Sludges, and Soils*; EPA: Washington, DC, 1996.
(46) Goertzen, S. L.; Thériault, K. D.; Oickle, A. M.; Tarasuk, A. C.; Andreas, H. A. Standardization of the Boehm Titration. Part I. CO2 Expulsion and Endpoint Determination. *Carbon N Y* **2010**, *48* (4), 1252−1261.
(47) Singh, A.; Srivastava, A.; Srivastava, P. C. Sorption-Desorption of Fipronil in Some Soils, as Influenced by Ionic Strength, PH and Temperature. *Pest Manag Sci.* **2016**, *72* (8), 1491−1499.
(48) Wang, J.; Guo, X. Adsorption Kinetic Models: Physical Meanings, Applications, and Solving Methods. *Journal of Hazardous Materials* **2020**, *390*, No. 122156. Elsevier B.V. May 15,
(49) Liu, C.; Yan, X.; Zhang, H. X.; Yang, J. m.; Yoon, K. B. Biochars and Modified-Biochars for Toxic-Metal/Metalloid Ions Sorption in Various Mixed Solution Systems: A Review on Kinetic and Isotherm Models. *Desalin. Water Treat.* **2024**, *319*, No. 100404.
(50) Chen, W.; Gong, M.; Li, K.; Xia, M.; Chen, Z.; Xiao, H.; Fang, Y.; Chen, Y.; Yang, H.; Chen, H. Insight into KOH Activation Mechanism during Biomass Pyrolysis: Chemical Reactions between O-Containing Groups and KOH. *Appl. Energy* **2020**, *278*, No. 115730.
(51) Sevilla, M.; Ferrero, G. A.; Fuertes, A. B. Beyond KOH Activation for the Synthesis of Superactivated Carbons from Hydrochar. *Carbon N Y* **2017**, *114*, 50−58.
(52) Raymundo-Piñero, E.; Azaïs, P.; Cacciaguerra, T.; Cazorla-Amorós, D.; Linares-Solano, A.; Béguin, F. KOH and NaOH Activation Mechanisms of Multiwalled Carbon Nanotubes with Different Structural Organisation. *Carbon N Y* **2005**, *43* (4), 786−795.
(53) Chen, W.; Yang, H.; Chen, Y.; Xia, M.; Chen, X.; Chen, H. Transformation of Nitrogen and Evolution of N-Containing Species during Algae Pyrolysis. *Environ. Sci. Technol.* **2017**, *51* (11), 6570−6579.
(54) Jain, A.; Tripathi, S. K. Fabrication and Characterization of Energy Storing Supercapacitor Devices Using Coconut Shell Based Activated Charcoal Electrode. *Materials Science and Engineering: B* **2014**, *183* (1), 54−60.
(55) Leng, L.; Huang, H.; Li, H.; Li, J.; Zhou, W. Biochar Stability Assessment Methods: A Review. *Science of the Total Environment* **2019**, *647*, 210−222.
(56) Falco, C.; Baccile, N.; Titirici, M. M. Morphological and Structural Differences between Glucose, Cellulose and Lignocellulosic Biomass Derived Hydrothermal Carbons. *Green Chem.* **2011**, *13* (11), 3273−3281.
(57) Huang, G. G.; Liu, Y. F.; Wu, X. X.; Cai, J. J. Activated Carbons Prepared by the KOH Activation of a Hydrochar from Garlic Peel and Their CO2 Adsorption Performance. *Xinxing Tan Cailiao/New Carbon Materials* **2019**, *34* (3), 247−257.
(58) Yu, X.; Liu, S.; Lin, G.; Yang, Y.; Zhang, S.; Zhao, H.; Zheng, C.; Gao, X. KOH-Activated Hydrochar with Engineered Porosity as Sustainable Adsorbent for Volatile Organic Compounds. *Colloids Surf., A* **2019**, *2020* (588), No. 124372. December
(59) Falk, G.; Shinhe, G. P.; Teixeira, L. B.; Moraes, E. G.; de Oliveira, A. P. N. Synthesis of Silica Nanoparticles from Sugarcane Bagasse Ash and Nano-Silicon via Magnesiothermic Reactions. *Ceram Int.* **2019**, *45* (17), 21618−21624.
(60) Fregolente, L. G.; de Castro, A. J. R.; Moreira, A. B.; Ferreira, O. P.; Bisinoti, M. C. New Proposal for Sugarcane Vinasse Treatment by Hydrothermal Carbonization: An Evaluation of Solid and Liquid Products. *J. Braz. Chem. Soc.* **2020**, *31* (1), 40−50.
(61) Carpanez, T. G.; Moreira, V. R.; Assis, I. R.; Amaral, M. C. S. Sugarcane Vinasse as Organo-Mineral Fertilizers Feedstock: Opportunities and Environmental Risks. *Science of the Total Environment. Elsevier B.V.* **2022**, *832*, No. 154998. August 1
(62) Laranja, M. J.; da Silva, R. C. J.; Bisinoti, M. C.; Moreira, A. B.; Ferreira, O. P.; Melo, C. A. Semivolatile Organic Compounds in the Products from Hydrothermal Carbonisation of Sugar Cane Bagasse and Vinasse by Gas Chromatography-Mass Spectrometry. *Bioresour. Technol. Rep.* **2020**, *12*, No. 100594.
(63) Ercan, B.; Alper, K.; Ucar, S.; Karagoz, S. Comparative Studies of hydrochars and Biochars Produced from Lignocellulosic Biomass via Hydrothermal Carbonization, Torrefaction and Pyrolysis. *Journal of the Energy Institute* **2023**, *109*, No. 101298.
(64) Fregolente, L. G.; Dos Santos, J. V.; Vinci, G.; Piccolo, A.; Moreira, A. B.; Ferreira, O. P.; Bisinoti, M. C.; Spaccini, R. Insights on Molecular Characteristics of hydrochars By13C-NMR and off-Line TMAH-GC/MS and Assessment of Their Potential Use as Plant Growth Promoters. *Molecules* **2021**, *26*, 1026.
(65) Perrone, O. M.; Colombari, F. M.; Rossi, J. S.; Moretti, M. M. S.; Bordignon, S. E.; Nunes, C.; da, C. C.; Gomes, E.; Boscolo, M.; Da-Silva, R. Ozonolysis Combined with Ultrasound as a Pretreatment of Sugarcane Bagasse: Effect on the Enzymatic Saccharification and the Physical and Chemical Characteristics of the Substrate. *Bioresour. Technol.* **2016**, *218*, 69−76.
(66) Sevilla, M.; Fuertes, A. B. Sustainable Porous Carbons with a Superior Performance for CO2 Capture. *Energy Environ. Sci.* **2011**, *4* (5), 1765−1771.
(67) Xiao, K.; Liu, H.; Li, Y.; Yang, G.; Wang, Y.; Yao, H. Excellent Performance of Porous Carbon from Urea-Assisted Hydrochar of Orange Peel for Toluene and Iodine Adsorption. *Chem. Eng. J.* **2019**, *2020* (382), No. 122997. August
(68) Thommes, M.; Kaneko, K.; Neimark, A. V.; Olivier, J. P.; Rodriguez-Reinoso, F.; Rouquerol, J.; Sing, K. S. W. Physisorption of Gases, with Special Reference to the Evaluation of Surface Area and Pore Size Distribution. *Pure and Applied Chemistry* **2015**, *87* (9−10), 1051−1069. (IUPAC Technical Report).
(69) Yu, X.; Liu, S.; Lin, G.; Yang, Y.; Zhang, S.; Zhao, H.; Zheng, C.; Gao, X. Promotion Effect of KOH Surface Etching on Sucrose-Based Hydrochar for Acetone Adsorption. *Appl. Surf. Sci.* **2019**, *496*, No. 143617. August
(70) Cychosz, K. A.; Thommes, M. Progress in the Physisorption Characterization of Nanoporous Gas Storage Materials. *Engineering* **2018**, *1*, 559−566.
(71) Zubbri, N. A.; Mohamed, A. R.; Lahijani, P.; Mohammadi, M. Low Temperature CO2capture on Biomass-Derived KOH-Activated Hydrochar Established through Hydrothermal Carbonization with Water-Soaking Pre-Treatment. *J. Environ. Chem. Eng.* **2021**, *9* (2), No. 105074.
(72) Tan, K. L.; Hameed, B. H. Insight into the Adsorption Kinetics Models for the Removal of Contaminants from Aqueous Solutions. *J. Taiwan Inst Chem. Eng.* **2017**, *74*, 25−48.
(73) Rathi, A.; Basu, S.; Barman, S. Adsorptive Removal of Fipronil from Its Aqueous Solution by Modified Zeolite HZSM-5: Equilibrium, Kinetic and Thermodynamic Study. *J. Mol. Liq* **2019**, *283*, 867−878.
(74) Gong, W.; Jiang, M.; Han, P.; Liang, G.; Zhang, T.; Liu, G. Comparative Analysis on the Sorption Kinetics and Isotherms of Fipronil on Nondegradable and Biodegradable Microplastics. *Environ. Pollut.* **2019**, *254*, 112927.
(75) Borges, M. M. C.; Pires, B. C.; Vieira, S. S.; Borges, K. B.; Guimarães, L. G. d. L. Magnetic and PH Responsive Composite Hydrogel-Based on Poly(2-(Diethylamino)Ethyl Methacrylate)/Chitosan for Fipronil Removal from Aqueous Medium. *React. Funct. Polym.* **2021**, *168*, No. 105050.

https://doi.org/10.1021/acssusresmgt.5c00321
ACS Sustainable Resour. Manage. 2025, 2, 1977−1985